



저작자표시-비영리-변경금지 2.0 대한민국

이용자는 아래의 조건을 따르는 경우에 한하여 자유롭게

- 이 저작물을 복제, 배포, 전송, 전시, 공연 및 방송할 수 있습니다.

다음과 같은 조건을 따라야 합니다:



저작자표시. 귀하는 원저작자를 표시하여야 합니다.



비영리. 귀하는 이 저작물을 영리 목적으로 이용할 수 없습니다.



변경금지. 귀하는 이 저작물을 개작, 변형 또는 가공할 수 없습니다.

- 귀하는, 이 저작물의 재이용이나 배포의 경우, 이 저작물에 적용된 이용허락조건을 명확하게 나타내어야 합니다.
- 저작권자로부터 별도의 허가를 받으면 이러한 조건들은 적용되지 않습니다.

저작권법에 따른 이용자의 권리는 위의 내용에 의하여 영향을 받지 않습니다.

이것은 [이용허락규약\(Legal Code\)](#)을 이해하기 쉽게 요약한 것입니다.

[Disclaimer](#)

High-dose-per-fraction radiation-induced
skin injury and underlying mechanism
of eosinophil-mediated skin fibrosis: An
animal model study



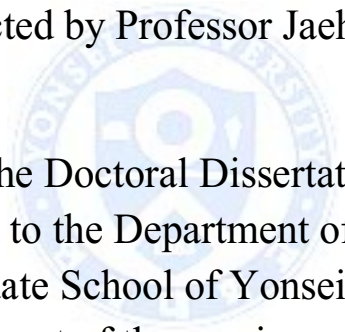
Jun Won Kim

Department of Medicine

The Graduate School, Yonsei University

High-dose-per-fraction radiation-induced skin injury and underlying mechanism of eosinophil-mediated skin fibrosis: An animal model study

Directed by Professor Jaeho Cho



The Doctoral Dissertation
submitted to the Department of Medicine,
the Graduate School of Yonsei University
in partial fulfillment of the requirements for the degree
of Doctor of Philosophy

Jun Won Kim

December 2015

This certifies that the Doctoral
Dissertation of Jun Won Kim is
approved.

Thesis Supervisor: Jaeho Cho

Thesis Committee Member#1: Won Jae Lee

Thesis Committee Member#2: Yun-Sil Lee

Thesis Committee Member#3: Se Hoon Kim

Thesis Committee Member#4: Yoon-Jin Lee

The Graduate School
Yonsei University

December 2015

ACKNOWLEDGEMENTS

I give thanks to God for allowing me to write this dissertation. I have a special debt of gratitude to my supervisor, Prof. Jaeho Cho for his knowledge, guidance and continuous support throughout the whole research project and completing this dissertation. I am also very grateful to Prof. Won Jae Lee, Prof. Yun-Sil Lee, Prof. Se Hoon Kim, and Dr. Yoon-Jin Lee for all the support and advice, which improved the quality of this work tremendously. I would like to extend my gratitude to Dr. Dong Won Lee and Dr. Eun-Jung Lee who provided their expertise in interpreting and publishing the data as well as in writing this dissertation. I would also like to thank Dr. Hyun Yoo and Ms. Jimin Lee for helpful discussion and technical assistance. Finally, I would like to thank my wife, Anna Kim, and three children, Joseph, Daniel, and Hope who gave me joy and meaning of life, and my parents and family in Canada who gave me continuous support and encouragement when I needed them the most.

December 2015

<TABLE OF CONTENTS>

ABSTRACT	1
I. INTRODUCTION	4
II. MATERIALS AND METHODS	8
1. Phase I. Development of mini-pig model for radiation-induced skin injury	8
A. Porcine skin irradiation	8
B. Skin toxicity assessment	9
C. Immunohistochemical analysis for skin microvasculature	10
D. Western blotting for IL-6 and TGF- β 1	11
2. Phase II. Mechanism of eosinophil-mediated skin fibrosis: single-fraction versus fractionated high-dose irradiation	12
A. Porcine skin irradiation	12
B. Mouse and cell irradiation	13
C. RNA-Seq analysis using mouse skin tissue	14
D. Cytokine detection	16
E. Cell migration assay	16
F. Statistical analysis	16
III. RESULTS	17
1. Phase I. Development of mini-pig model for radiation-induced skin injury	17
A. Gross and histologic changes of the porcine skin after high-dose irradiation in single fraction	17
B. Spectrophotometric analysis of skin damage	19
C. Dose-dependent changes in microvessel density - CD31	21
D. Western blot assay for IL-6 and TGF- β 1	22
2. Phase II. Mechanism of eosinophil-mediated skin fibrosis: single-fraction versus fractionated high-dose irradiation	23

A. 30 Gy in single-fraction induced higher expression of fibrosis-related factors and eosinophil recruitment in porcine skin than 30 Gy in 5 fractions	23
B. Upregulation of eosinophil-related factors following irradiation	26
C. IL-33 induction in mouse skin following 30 Gy in single fraction	28
D. Eosinophil-mediated Th2 immune reaction by IL-33 secreted from impaired vascular endothelial cells in the skin.....	30
IV. DISCUSSION	34
V. CONCLUSION	41
REFERENCES	42
ABSTRACT (IN KOREAN)	48
PUBLICATION LIST	51



LIST OF FIGURES

Figure 1. Experimental design, Phase I.....	9
Figure 2. Experimental design, Phase II.....	12
Figure 3. Skin response to single-fraction high-dose irradiation ..	18
Figure 4. Correlation between radiation dose and number of eosinophils in the dermis	19
Figure 5. Spectrophotometry data	20
Figure 6. Changes in % of original area of microvessel lumen per high-power field after 15–75 Gy irradiation	22
Figure 7. Protein expression of IL-6 and TGF- β 1 after irradiation of 15–30 Gy	23
Figure 8. 30 Gy in single fraction induces enhanced production of profibrotic factors compared to 30 Gy in 5 fractions.....	25
Figure 9. IL-6 expression in porcine skin irradiated with 30 Gy in single or 5 fractions.....	26
Figure 10. Upregulation of eosinophil-related factors in porcine skin by 30 Gy in single fraction vs. 5 fractions	27
Figure 11. Enrichment of granulocyte adhesion and upregulation of IL-33	29
Figure 12. Production of IL-33 and blood vessel damage by high-dose irradiation in single fraction	32
Figure 13. Schematic model of the signaling pathway involved in the eosinophil-mediated immune response and fibrosis induced by high-dose radiation in the skin	40

LIST OF TABLES

Table 1. Radiation Therapy Oncology Group toxicity grading	10
Table 2. The porcine and mouse primer sequences	15



ABSTRACT

High-dose-per-fraction radiation-induced skin injury and underlying mechanism of eosinophil-mediated skin fibrosis: An animal model study

Jun Won Kim

*Department of Medicine
The Graduate School, Yonsei University*

(Directed by Professor Jaeho Cho)

Objective: Normal tissue injury due to hypofractionated ablative radiotherapy differs from tissue response to conventional-fractionation radiotherapy. Using animal models, dose-dependent skin response to high-dose-per-fraction radiation is characterized, and underlying mechanism of eosinophil-mediated skin fibrosis is investigated.

Methods: In Phase I, the dorsal skin of a mini-pig was irradiated with electron beam of 15, 30, 50 and 75 Gy in single fraction. Gross skin changes were quantitatively assessed using spectrophotometer, and histologic changes were documented through full-thickness skin biopsies performed serially during 12-week observation. Changes in vasculature with CD-31 staining and IL-6 and TGF- β 1 expression through Western blotting were characterized. In Phase II,

the dorsal skin of a mini-pig was irradiated with 30 Gy in single fraction and 30 Gy in 5 fractions. Eosinophil-related Th2 cytokines were evaluated using quantitative real-time PCR. RNA-sequencing using mouse skin irradiated with 30 Gy in single fraction and functional assays using a co-culture system of THP-1 cells and irradiated-human umbilical vein endothelial cells (HUVECs) were performed to investigate the mechanism of eosinophil-mediated radiation skin fibrosis.

Results: A 4-week latency period was followed by the usual course of erythema, dry desquamation, moist desquamation, and ulceration, while irreversible skin ulceration and necrosis was observed after receiving ≥ 50 Gy. The number of eosinophils began rising sharply at 4 weeks and normalized after reaching a peak at 7-8 weeks. Changes in microvessel density showed a biphasic pattern with a transient peak at 1 week, a nadir at 4-6 weeks, and maximum recovery at 9 weeks. Increase in the level of IL-6 and TGF- β 1 was detected soon after irradiation. In comparison with 30 Gy in 5 fractions, 30 Gy in single fraction caused more pronounced eosinophil accumulation, increased level of profibrotic factors including collagen and TGF- β , enhanced production of eosinophil-related cytokines including IL-4, IL-5, CCL11, IL-13, and IL-33, and reduction in vessel density. Level of IL-33 notably increased in the vessels of pig and mouse skin after 30 Gy in single fraction, as well as in HUVECs following 12 Gy in single fraction. Blocking IL-33 suppressed the migration ability of THP-1 cells and cytokine secretion in a co-culture system of THP-1

cells and irradiated HUVECs.

Conclusions: Our porcine skin model provides an effective platform for studying skin injury due to high-dose-per-fraction irradiation. High-dose-per-fraction irradiation appears to enhance eosinophil-mediated fibrotic responses, and IL-33 may be a key molecule operating in eosinophil-mediated skin fibrosis.



Key Words: radiation-induced skin injury; porcine skin injury model; high-dose-per-fraction irradiation, eosinophil-mediated fibrosis, interleukin-33

High-dose-per-fraction radiation-induced skin injury and underlying mechanism of eosinophil-mediated skin fibrosis: An animal model study

Jun Won Kim

*Department of Medicine
The Graduate School, Yonsei University*

(Directed by Professor Jaeho Cho)

I. INTRODUCTION

Ionizing radiation causes tumor cell death as well as acute and late toxicities to surrounding normal tissues. Skin is usually the first site of entry in radiation treatment, and various degrees of skin reactions can occur. Interest in hypofractionated ablative radiotherapy, which may potentiate normal tissue injury, has increased lately with improvements in radiation delivery technology and image guidance, and its clinical applications are increasing for treating various tumor sites including brain, bone, lung, liver, and the breast. There are concerns for increased acute and late toxicities that were not apparent with conventional schedules. Using the linear-quadratic model, which is based on biologically equivalent dose from conventionally fractionated treatments to the tissue, to establish normal tissue dose limits may not apply to large fraction sizes (i.e., >8

Gy/fraction). Above this dose range, cells may have significantly less ability to repair DNA damage. Radiation-induced skin toxicity becomes progressively more significant with increasing dose per fraction. Late-responding tissues (fibroblasts and endothelial cells) are more affected by increasing dose per fraction than early-responding tissues such as skin basal cells. Skin toxicity is of particular concern for breast cancer patients, since skin is often in close proximity to or even within the irradiation field. Accelerated partial breast irradiation delivers a high-dose-per-fraction to the tumor cavity and adjacent breast tissue in 1-10 fractions. Increased acute (acute radiation dermatitis and desquamation) and late (delayed wound healing, ulceration, necrosis, telangiectasia, fibrosis, and poor cosmetic outcome) effects are observed with high skin dose.¹ Early results from stereotactic body radiotherapy (SBRT) for early lung cancer also have reported increased skin toxicity.²

Degrees and characteristics of radiation-induced skin injury depend on a variety of factors including total radiation dose, size of fractional dose, type and quality of radiation, and irradiated skin volume.³ Severe radiation-induced skin injuries can cause severe pain, deformation, secondary infection, ulcers and even necrosis when intolerable doses are administered,⁴ and quality of life for these patients is diminished considerably. Deregulation of normal regenerative responses to physical, chemical and biological toxins leads to abnormal remodeling of extracellular matrix with pathological fibrosis. Processes deregulated after radiotherapy have much in common with processes associated

with fibrotic diseases affecting the heart, skin, lungs, kidneys, gastrointestinal track and liver. However, the mechanisms underlying radiation-induced fibrosis are not clearly understood. Irradiation can induce cytokine and chemokine production that leads to fibrosis and polarized immune responses.^{5,6} Abnormal immune reactions such as inflammation and polarized immune responses may in turn be involved in fibrosis.⁷ Among the secreted factors driving fibrosis, transforming growth factor beta 1 (TGF- β 1) produced by a wide range of inflammatory, mesenchymal and epithelial cells converts fibroblasts and other cell types into matrix-producing myofibroblasts. Eosinophils were reported to play a major role in pulmonary fibrosis⁸ by triggering Th2-polarized immune reactions.⁹ Th2 immune response has been associated with upregulation of Th2-type cytokines including IL-4, IL-5, IL-10, and IL-13 and induction of mast cells.^{10,11} Highly polarized Th2 cytokine responses are also closely related to progression of fibrosis.¹²

One of the main uncertainties is the relevance of very early events, including inflammatory responses in blood vessels, to fibrosis. IL-33, a recently discovered member of the IL-1 cytokine family, is constitutively expressed in epithelial barrier tissues, such as skin, where it is found preferentially localized to the nucleus of epithelial and endothelial cells. Increased expression of IL-33/IL-33R has been correlated with fibrotic disorders, such as scleroderma and progressive systemic sclerosis. IL-33 potently stimulates secretion of Th2 cytokines such as IL-5 and IL-13 by ST2-expressing immune cells, which

contribute to the development of Th2 immune responses.^{13,14} Administration of IL-33 to mice resulted in increased serum levels of Th2 cytokines including IL-4, IL-5, and IL-13, as well as IgG1 and IgE, and inflammation was accompanied by eosinophil accumulation in the lung and gut.¹⁵ IL-33 also induces cutaneous fibrosis via eosinophil-derived IL-13 and lung fibrosis through type-2 macrophage-induced IL-13 and TGF- β .^{16,17}

Unfortunately, no preventive measure or effective treatment for radiation-induced skin injury is currently available except for conservative management. Thus, effective strategy to prevent and treat radiation-induced skin injury is urgently requested in the modern radiotherapy era.

In Phase I of the current study, we developed a porcine skin model in order to investigate radiation-induced skin injury using high-dose electron beam delivered in single fraction. 15 Gy, 30 Gy, 50 Gy, and 75 Gy in single fraction was used in order to determine the dose-dependent response of the porcine skin as well as the maximum radiation dose that our pig skin model could tolerate without irreversible skin damage. In Phase II, we investigated the underlying mechanism of eosinophil-associated skin fibrosis and the effects of high-dose-per-fraction radiation, using maximum tolerable dose (MTD) determined from Phase I study.

II. MATERIALS AND METHODS

1. Phase I. Development of mini-pig model for radiation-induced skin injury

A. Porcine skin irradiation

The study design was approved by the Institutional Animal Care and Use Committees. A female Micro-pig® (Medi Kinetics Co, Ltd., Pyeongtaek, Korea) weighing 25 kg was anesthetized with intravenous injections of Zoletil (tiletamine and zolazepam) 0.1cc/kg and Rompun (xylazine) 0.1cc/kg. The pig's entire skin was scanned with computed tomography, and the maximum epidermal/dermal thickness was determined to be less than 2 cm (Figure 1A). By varying the thickness of the lead shielding (1, 2, and 3 mm), film dosimetry determined the appropriate shielding thickness (3 mm) (Figure 1B). The pig's dorsal skin was divided into 4 sections. A lead shield containing 11 cut-out squares, 2 cm × 2 cm in size and at least 2.5 cm from each other, was placed over one section of the dorsal skin. A single fraction of 15, 30, 50 or 75 Gy with 6-MeV electrons was delivered to each section of the dorsal skin using a linear accelerator (Elekta, Stockholm, Sweden), ensuring that greater than 90% of the prescribed dose would be limited to a maximum depth of 2 cm (Figure 1C-D).

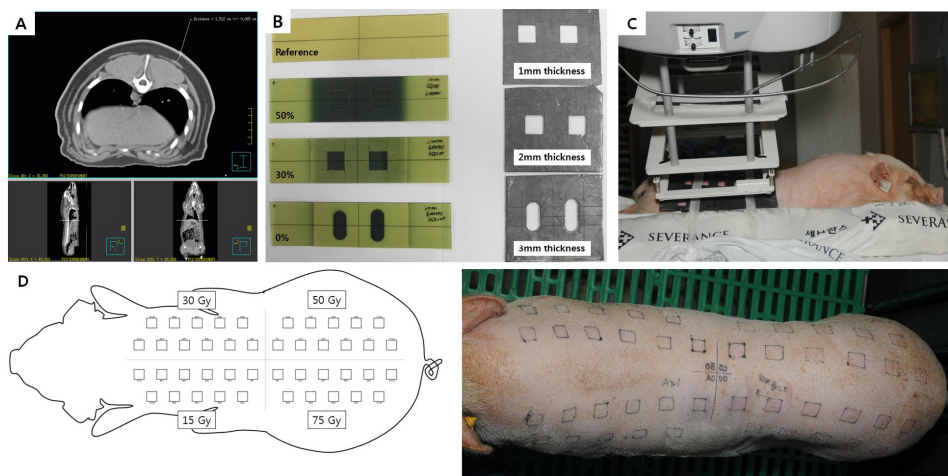


Figure 1. Experimental design, Phase I. (A–B) The thickness of the pig’s skin was measured using CT, and appropriate thickness (3 mm) of the lead cutout was determined using film dosimetry. (C–D) The pig’s dorsal skin was divided into 4 sections. A lead shield containing 11 cut-out squares, 2 cm × 2 cm in size, was placed over the skin. A single fraction of 15, 30, 50 or 75 Gy with 6-MeV electrons was delivered to each section of the skin using a linear accelerator.

B. Skin toxicity assessment

The pig was housed and observed for 12 weeks to allow acute and late effects of radiation to develop. The 4 squares located in the center of the dorsal skin, each of which was irradiated with a different dose, were left for weekly observation for gross skin changes and spectrophotometric analysis until the 12th week. Radiation Therapy Oncology Group (RTOG) toxicity grading¹⁸ was used for the assessment of the gross skin reaction after irradiation (Table 1). Changes in the skin color

were assessed weekly using a portable spectrophotometer (CM-700d, Konica Minolta Sensing Inc., Osaka, Japan), and melanin and erythema indices were recorded. The melanin index (M) is defined as $M = 100 \times \log (1/\text{intensity of reflected red light})$, and the erythema index (E) is defined as $E = 100 \times \log (\text{intensity of reflected red light} / \text{intensity of reflected green light})$.¹⁹

Table 1. Radiation Therapy Oncology Group toxicity grading

	Grade 0	Grade 1	Grade 2	Grade 3	Grade 4
Acute	None	Follicular, faint or dull erythema / epilation / dry desquamation / decreased sweating	Tender or bright erythema, patchy moist desquamation / moderate edema	Confluent, moist desquamation other than skin folds, pitting edema	Ulceration, hemorrhage, necrosis
Chronic	None	Slight atrophy; pigmentation change; some hair loss	Patch atrophy; moderate telangiectasia; total hair loss	Marked atrophy; gross telangiectasia	Ulceration

C. Immunohistochemical analysis for skin microvasculature

Two of the 44 fields were biopsied at 1st, 2nd, 4th, 6th, and 9th week for each radiation dose. The 4 fields that were left for observation were biopsied at 12th week. Each biopsied specimen consisted of a full-thickness block (1.5 cm x 0.5 cm) within the irradiated field. A half of the block was fixed in 10% neutral buffered formalin, and the other half was frozen in liquid nitrogen for Western blot analysis. Formalin-fixed biopsy samples were embedded in paraffin, sectioned, and then examined histologically. The 5- μ m sections from each biopsy specimen were stained with anti-CD31 monoclonal antibody for pig (Abcam, Cambridge,

UK) to determine microvessel density according to a standard three-step immunohistochemical procedure.²⁰ Each section was examined microscopically and the cross-sectional area of the positively-stained vessel lumens were measured in five high-power fields (HPF) per slide (magnification x200), and average values were obtained. Within-group and between-group means were compared, and significance was detected with a two-tailed t test.

D. Western blotting for IL-6 and TGF- β 1

The frozen tissue samples were homogenized in RIPA lysis buffer (150 mM sodium chloride, 0.5% Triton X-100, 0.5% sodium deoxycholate, 0.1% sodium dodecyl sulfate (SDS), 50 mM Tris, pH 8.0) that contained protease inhibitors. The lysates were then centrifuged at 13,000 rpm at 4 °C for 5 minutes and separated on SDS-PAGE. The proteins were transferred to a polyvinylidene fluoride (PVDF) membrane (Millipore, MA, USA) and then incubated overnight with antibodies and detected with ECL (ECL Western Blotting Substrate, Pierce, USA) following treatment with 5% milk powder in Tris buffered saline (TBS) to prevent non-specific reactions. The specific antibodies used for this experiment were rabbit anti-IL-6 (Abcam, Cambridge, UK), rabbit anti-TGF- β 1 (Abcam, Cambridge, UK) and mouse anti- α -tubulin (Abcam, Cambridge, UK). Each dried blot was scanned and saved as a Tagged Image File Format (TIFF) file, and the density of the corresponding band was quantified using Image J, a Java-based image processing software (U.S. National Institutes of Health, Bethesda,

Maryland; downloaded from <http://imagej.nih.gov/ij/>).²¹ Values are expressed as the relative intensity to α -tubulin.

2. Phase II. Mechanism of eosinophil-mediated skin fibrosis: single-fraction versus fractionated high-dose irradiation

A. Porcine skin irradiation and biopsy

The radiation-induced porcine skin injury model in Phase I determined the maximum tolerable dose.²² The dorsal skin was divided into two sections, and 30 Gy in a single fraction and 30 Gy in 5 fractions with a 6-MeV electron beam were delivered to each side of the dorsal skin. The pig was housed and observed for 14 weeks to allow acute and late effects of radiation to develop (Figure 2).

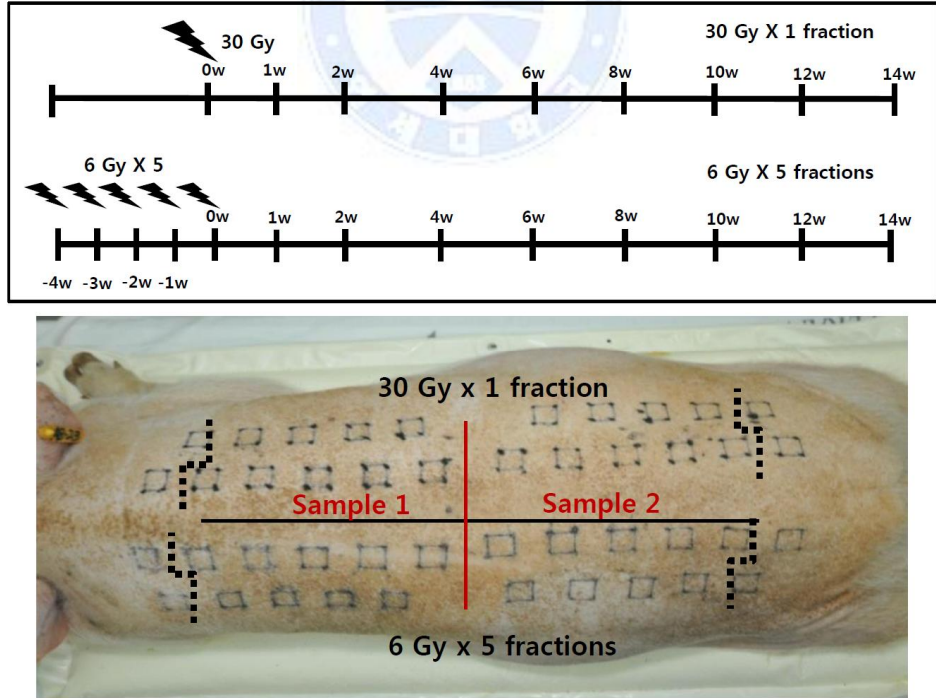


Figure 2. Experimental design, Phase II. (A) Schedule of irradiation. (B) The pig's dorsal skin was divided into 2 sides. A lead shield containing cut-out squares, 2 cm \times 2 cm in size, was placed over the skin. 30 Gy in single and 30 Gy in 5-fractions was delivered to each side of the dorsal skin.

B. Mouse and cell irradiation

Procedures described by Yoo et al. were followed for mouse and cell irradiation.²³ Radiation was delivered with an X-RAD 320 X-ray unit (Precision, North Branford, USA) equipped with fixed and adjustable collimators. For mouse skin irradiation, the collimators produced a beam with a 1 cm \times 1 cm coverage area. The percentage depth doses (PDDs) were determined after absolute dosimetric measurements with Gafchromic EBT3 film, and acrylic and water-equivalent RW3 slab phantoms (PTW, RW3). The dose rate of the aluminum-filtered X-ray beam was 8.3 cGy/s, measured at 320 kV and 12.5 mA using a cylindrical Farmer-type ionization chamber (PTW 0.6 cm², waterproof) placed in an RW3 phantom at a source-to surface distance of 2cm. The output was calibrated as recommended by the American Association of Physicists in Medicine, TG-61 report.²⁴ Using the 1 cm \times 1 cm collimator, the flank skin of 6 mice was irradiated with a single dose of 30 Gy.

Radiation dosimetry for cultured cells was carried out using a cell culture dish, water, an RW3 phantom slab, and Gafchromic EBT3 film. The cell culture dishes were filled with 10 mL water. EBT3 film was placed in the bottom of each

dish for radiation measurement. Radiation delivered to the EBT3 films was converted to dose value using a PDD calibration curve (optical density-pixel value plotted against radiation dose in cGy). Cells were irradiated with 12 Gy and 4 Gy in single fractions.

C. RNA-Seq analysis using mouse skin tissue

To reveal what factors promote eosinophil recruitment in irradiated skin, we performed RNA-Seq using mouse skin samples with and without 30 Gy-irradiation in single fraction. Total RNAs were isolated using TRIzol (Invitrogen, CA), and mRNA was isolated from total RNAs using oligo-dT beads. Construction and sequencing of an RNA-Seq library were performed based on Illumina HiSeq2000 protocols to generate 101 paired-end RNA-Seq reads. The quality of raw data was checked using FastQC,²⁵ and the adaptor sequences of the Illumina sequencing platform were trimmed using Trimmomatic (ILLUMINACLIP:2:30:10 MINLEN:75) before read alignment. All quality-filtered reads were aligned to the *Mus musculus* genome (GRCm38) from the Ensembl database (release 73) using Tophat.²⁶ Aligned reads were sorted using SAMtools,²⁷ and the read count for each gene was calculated using HTseq.²⁸ To identify differentially expressed genes between the two conditions, we used the R package DESeq,²⁹ which is based on a negative binomial model. Based on the differentially expressed genes (DEGs) identified using DESeq ($P < 0.01$, Bonferroni corrected), we conducted Ingenuity Pathway Analysis (Qiagen, Hilden,

Germany). Endothelial cells, epithelial cells, dermis, and epidermis were selected to conduct the core analysis in Ingenuity Pathway Analysis, and other options were set to default.

Total RNA was isolated from tissue using TRIzol reagent (Invitrogen, CA). Real-time PCR analysis was performed using an ABI real-time analyzer (Corbett Life Science, Australia) to measure SYBR Green (Qiagen, Hilden, Germany). Relative amounts of mRNA were normalized to actin mRNA levels within each sample. A reverse transcription system for cDNA synthesis and the primer sets for IL-13 were purchased from Qiagen (Hilden, Germany). The porcine and mouse primer sequences were described in Table 2. The amplification program consisted of 1 cycle of 95°C with a 10-min hold, followed by 35 cycles of 95°C with a 20-second hold, 60°C with a 20-second hold, and 72°C with a 20-second hold. After normalization with actin, the median target level in non-irradiated skin was used as a calibrator.

Table 2. The porcine and mouse primer sequences

Porcine	primer sequences
TGF-β1	F-5'-GAACAAACTCTTGGGCAATG-3', R-5'- ACTTCCAGCTTGTCACCTTG-3
IL-33	F-5'-GTAAACCTGAGCCCCACAAA-3', R-5'-TTGAATCCTCAGGGTGTTCC-3'
IL-4	F-5'-TCTCACCTCCCAACTGATCC-3', R-5'-AGCTCCATGCACGAGTTCTT-3'
CCL11	F-5'-CCAAAGAGTCACTGCCAACA-3', R-5'-ACTCCATGGCATTCTGAACC-3'
IL-5	F-5'- GATAGGCGATGGGAACCTGA-3', R-5'- CCCTCGTGCAGTTTGATTCT-3'
β-actin	F-5'-TGCCCCCATGTTTGTGATG-3', R-5'-TGCCCCCATGTTTGTGATG-3'
Mouse	primer sequences
IL-33	F-5'-ATTTCCCCGGCAAAGTTCAG-3', R-5'- AACGGAGTCTCATGCAGTAGA-3'
GAPDH	F-5'- CATCACTGCCACCCAGAAGA-3', R-5'- CAGATCCACGACGGACACAT-3'

D. Cytokine detection

IL-4, IL-6, and IL-33 proteins were measured in culture supernatants by ELISA. ELISAs were performed using specific monoclonal antibody pairs for the detection of both IL-6 and IL-4 (BD Bioscience, CA). ELISA for IL-33 detection was performed using the DuoSet human IL-33 ELISA kit (R&D Systems, MN).

E. Cell migration assay

FluoroBlok™ inserts with 8-μm pores (Corning Life Science, Tewksbury, MA) and 24-well plates were assembled as upper and lower chambers, and 5×10^5 THP-1 cells were placed in the upper chamber in the presence of 12 Gy-irradiated human umbilical vein endothelial cells (HUVECs) for 48 h. At the end of incubation, cells in the upper chamber were removed with cotton swabs, and cells that traversed the membrane to the lower surface of the insert were fixed with 4% paraformaldehyde. Fixed cells were stained with Hoechst 33342 (Thermo Scientific, Pittsburgh, PA) and evaluated spectrophotometrically using a microplate reader (Synergy H4 hybrid reader, BioTek).

F. Statistical analysis

Data are presented as mean \pm SD, and groups were statistically compared using the unpaired 2-sided Student's t-test. All experiments were performed at least three times. $P < 0.05$ (*) and $P < 0.01$ (**) were considered statistically significant.

III. RESULTS

1. Phase I. Development of mini-pig model for radiation-induced skin injury

A. Gross and histologic changes of the porcine skin after high-dose irradiation in single fraction

Figure 2 summarizes the gross and histologic changes of the skin after a single fraction irradiation of 15 Gy, 30 Gy, 50 Gy, or 75 Gy, observed at 0-12 weeks post-irradiation. Transient erythema occurred within 1 week in the fields irradiated with 50 and 75 Gy, and it was followed by a 4-week period of latency during which no definite skin reaction was observed. Erythema and dry desquamation (RTOG grade 1), moist desquamation (grade 3), and ulceration (grade 4) appeared 4, 6 and 9 weeks after irradiation, respectively. Fields receiving 15 Gy and 30 Gy healed without ulceration, while irradiation ≥ 50 Gy resulted in ulceration followed by necrosis (Figure 3A). A plot of gross skin changes according to RTOG grading of acute skin toxicity against time after irradiation showed skin changes were more pronounced and occurred early with increasing radiation dose (Figure 3D). Figures 3B-C show histologic evaluation of full-thickness biopsy specimens after 30 Gy (H&E, magnification x100 and x400, respectively). The changes in the epidermal layer corresponded to those of the gross skin. Interestingly, the average number of eosinophils per HPF rose sharply after 4 weeks, peaked at 7-8 weeks and disappeared at 12 weeks post-irradiation. Degranulation from eosinophils was apparent 9 weeks after irradiation. Figure 4 shows patterns of eosinophil infiltration in the intra- and perivascular spaces of the

dermis biopsied 4 weeks (A) and 9 weeks (B) after 30-Gy irradiation as well as the average number of eosinophils in five HPF (magnification, x400) from tissue sections irradiated with 15-75 Gy (C). The rate of increase and the peak in the eosinophil count was markedly pronounced after 75 Gy. Induction of eosinophilia seemed to coincide with the acute and subacute skin response to radiation.

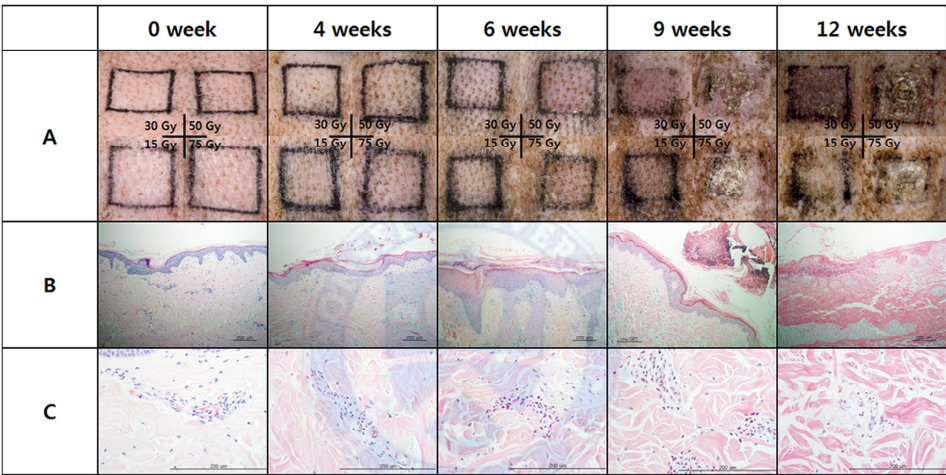


Figure 3. Skin response to single-fraction high-dose irradiation. (A) Gross skin changes in 15, 30, 50 and 75 Gy fields. Erythematous changes, wet desquamation

and ulceration began to appear 4, 6 and 9 weeks after irradiation, respectively. (B–C) Histologic evaluation of full-thickness biopsy specimens after 30 Gy (H&E, magnification $\times 100$ and $\times 400$). (D) Gross skin changes according to RTOG grading of acute skin toxicity are plotted against time after irradiation.

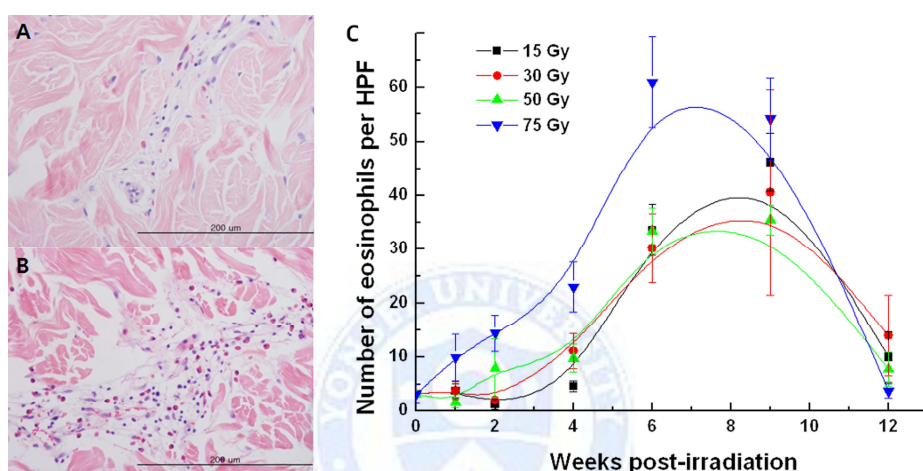


Figure 4. Correlation between radiation dose and number of eosinophils in the dermis. Representative sections from the skin irradiated with 30 Gy, biopsied (A) 4 weeks after irradiation, and (B) 9 weeks after irradiation (magnification, $\times 400$). (C) The mean numbers of eosinophils in 5 high-powered fields (magnification, $\times 400$) from a tissue section irradiated with 15–75 Gy are plotted against time.

B. Spectrophotometric analysis of skin damage

Figure 5 shows changes in the mean values of melanin and erythema indices in the porcine skin that received 15 and 30 Gy, from the time of irradiation to 12 weeks post-irradiation. The melanin indices for 15 Gy began increasing sharply from

0.35 at 6 weeks to a peak value of 0.95 at 10 weeks and decreased to a baseline level of 0.43 at 12 weeks post-irradiation. The melanin indices for 30 Gy were 0.29, 0.80, and 1.04 at 6, 10, and 12 weeks, respectively. The pattern of changes in melanin indices closely resembled progression of gross changes in the skin after high dose (≥ 50 Gy) irradiation. The erythema indices for the 15 Gy showed early and continuous increase from 0.8 at 1 week to a peak of 2.1 at 9 weeks and decreased to 1.8 at 12 weeks post-irradiation. Changes in the erythema indices for 30 Gy showed a close resemblance to those of 15 Gy. This result was in sharp contrast to that of the gross skin reactions, which did not show erythematous changes until 4 weeks after irradiation. The areas of the skin irradiated with 50 and 75 Gy showed ulceration and necrosis 6 weeks after irradiation and were not available for spectrophotometric analysis.

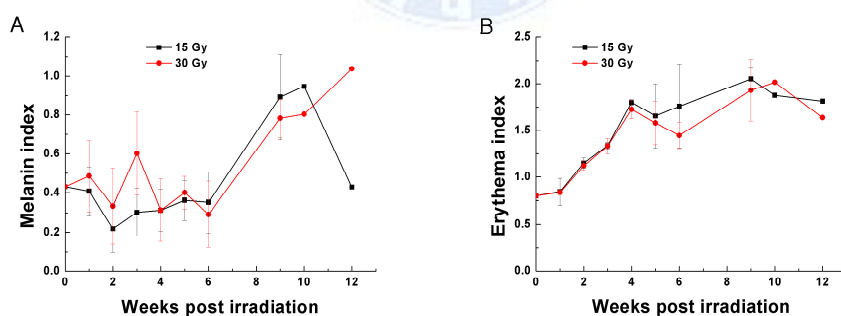


Figure 5. Spectrophotometry data. (A) The mean value of melanin indices is plotted against time post-irradiation. Melanin indices began rising 6 weeks after irradiation. (B) The mean value of erythema indices is plotted against time

post-irradiation. Erythema indices began rising soon after irradiation and continued to increase.

C. Dose-dependent changes in microvessel density - CD31

Figure 6 shows changes in the density of dermal microvessels after irradiation with 15-75 Gy. Microvessel density showed a biphasic pattern with a transient peak at 1 week, a nadir at 4-6 weeks, and maximum recovery at 9 weeks. The density in the 15-Gy field showed full recovery 12 weeks after irradiation. On the other hand, microvessel density in the 30-75 Gy fields recovered to maximum values at 9 weeks post-irradiation and decreased towards the end of observation. Microvessel density from 50- and 75-Gy fields showed lower initial transient peaks and lower nadirs at earlier time points compared with the values from 15- and 30-Gy fields. The initial peaks (at 1-week post-irradiation) for microvessel density showed significant differences ($p < 0.0001$) between each experimental group irradiated with different doses, while the differences in the nadir (at 4-week post-irradiation) for different dose levels were not significant ($p = 0.660$). During the latency period of 0-4 weeks, the changes in the microvessel density were substantial.

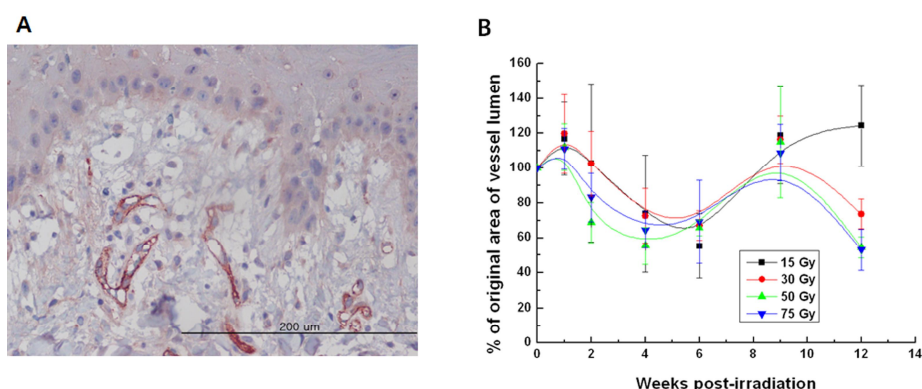


Figure 6. Changes in % of original area of microvessel lumen per high-power field after 15–75 Gy irradiation. (A) A representative section from the skin irradiated with 30 Gy and biopsied 6 weeks after irradiation was stained with antibody to CD31 (magnification, $\times 400$). (B) The density of CD31-stained small arterioles was determined by summing the luminal areas of microvessels in each high-powered field (magnification, $\times 200$). The mean density of 5 HPFs for each section was compared with the baseline value obtained on Day 0 and is expressed as a percentage.

D. Western blot assay for IL-6 and TGF- $\beta 1$

Figure 7 shows sequential expression of IL-6 (A-B) and TGF- $\beta 1$ (C-D) after irradiation of 15–30 Gy. Expression of IL-6 and TGF- $\beta 1$ increased after 30-Gy irradiation compared with 15-Gy irradiation. Increase in the level of IL-6 for higher dose (30 Gy) was detected soon after irradiation with an earlier peak compared with the values for lower dose (15 Gy). Levels of TGF- $\beta 1$ began increasing soon after irradiation and persisted throughout observation period.

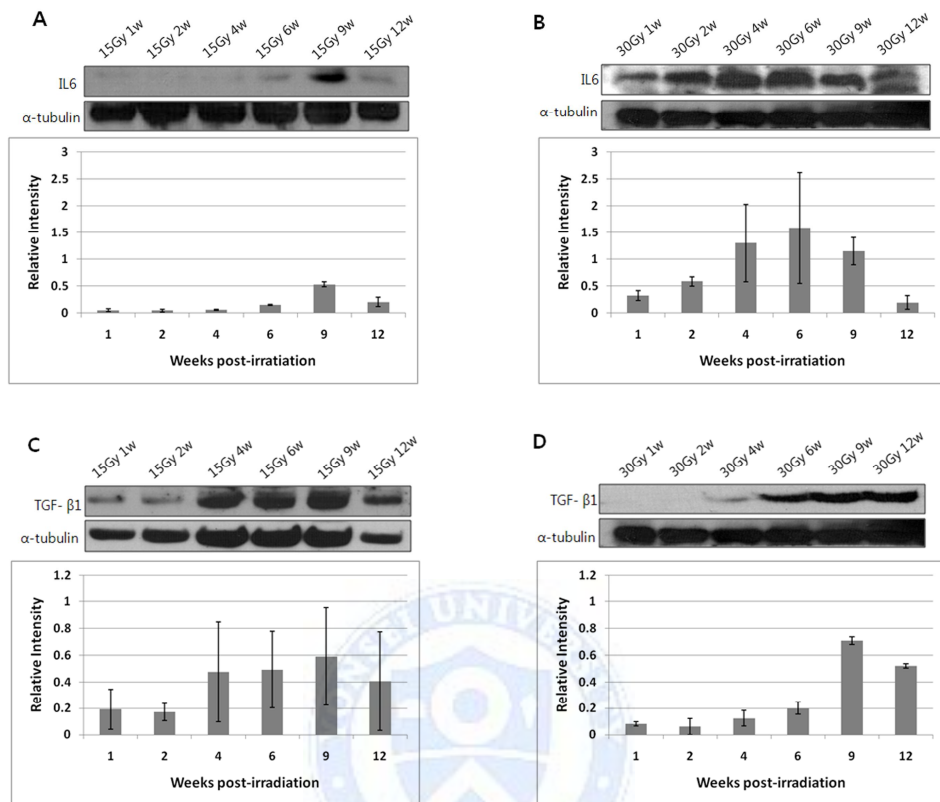


Figure 7. Protein expression of IL-6 (A–B) and TGF- β 1 (C–D) after irradiation of 15–30 Gy. Western blot analyses were performed, and density of the corresponding bands was quantified using Image J 1.37v analysis software. Values are expressed as the relative intensity compared with α -tubulin.

2. Phase II. Mechanism of eosinophil-mediated skin fibrosis: single-fraction versus fractionated high-dose irradiation

A. 30 Gy in single-fraction induced higher expression of fibrosis-related factors and eosinophil recruitment in porcine skin than 30 Gy in 5 fractions

The maximum tolerable dose without overt ulceration of porcine skin was determined to be 30 Gy in single fraction in Phase I study.²² Here, we investigated the effect of 30 Gy in single fraction on fibrosis-related factors and eosinophils compared with 30 Gy in 5 fractions (Figure 2). Figure 8 shows radiation-induced histological changes in the porcine skin. Histological examination of biopsy specimens indicated that high-dose irradiation of 30 Gy in single fraction induced more epidermal hyperplasia, collagen accumulation, and α -SMA expression than 30 Gy in 5 fractions at 14 weeks (Figure 8a-c). Additionally, TGF- β mRNA and protein expression was more pronounced by single high-dose irradiation than fractionated irradiation (Figure 8d). In Phase I study, we demonstrated that inflammatory responses including IL-6 expression and eosinophil infiltration were increased in irradiated porcine skin.²² IL-6 expression was enhanced in both fractionation schemes, with no significant difference between the two schemes (Figure 9). The average number of eosinophils was determined in five high-power fields (magnification, $\times 400$) in irradiated tissue sections, and the rate of increase and peak eosinophil counts were more pronounced after 30 Gy in single fraction compared with 30 Gy in 5 fractions (Fig. 8e). The average number of eosinophils increased sharply after 2 weeks, peaked at 6 weeks, and subsided to baseline levels at 12 weeks after 30 Gy in single fraction. Induction of eosinophils appeared to coincide with the acute and subacute skin response to radiation.

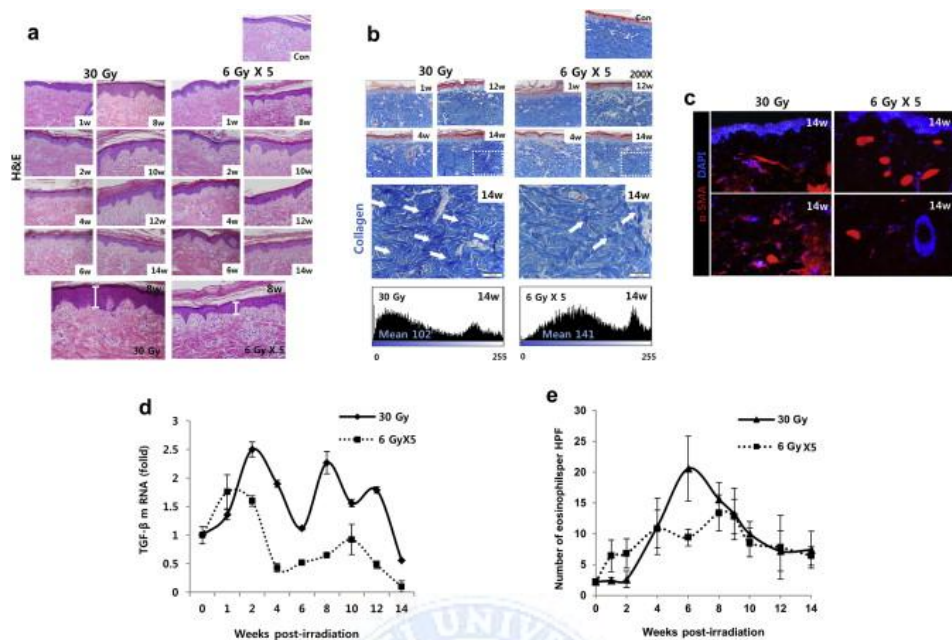


Figure 8. 30 Gy in single fraction induces enhanced production of profibrotic factors compared with 30 Gy in 5 fractions. Areas of porcine skin subjected to 30 Gy in single fraction and 30 Gy in 5 fractions were biopsied at the indicated times and stained with H&E, Masson's trichrome, and TGF- β and α -SMA antibodies. mRNA was isolated from biopsy specimens for qRT-PCR. (a) Histology, (b) collagen deposition, (c) α -SMA expression, (d) TGF- β mRNA and protein expression, and (e) the mean numbers of eosinophils in 5 high-power fields (magnification, $\times 400$) from tissue sections irradiated with 30 Gy in single fraction and 30 Gy in 5 fractions are plotted against time.

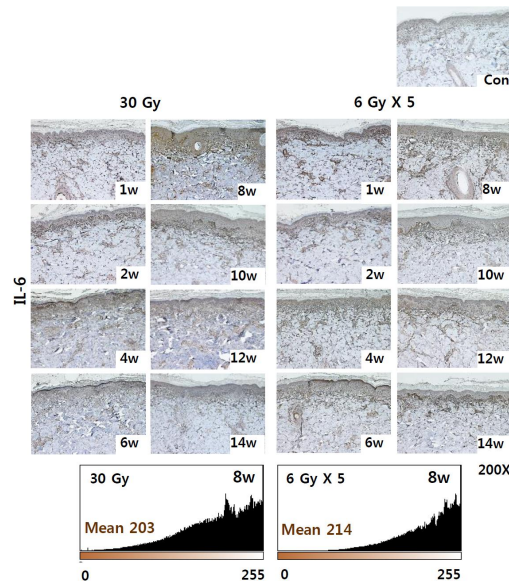


Figure 9. IL-6 expression in porcine skin irradiated with 30 Gy in single or 5 fractions.

B. Upregulation of eosinophil-related factors following irradiation

Since eosinophils can regulate Th2 immunity,⁹ eosinophil-related Th2 cytokines such as IL-4, IL-5, and CCL11 (eotaxin) were evaluated by quantitative real-time PCR (qRT-PCR). Increases in IL-4, CCL11, and IL-5 mRNA levels were more pronounced after 30 Gy in single fraction (Fig. 10a-c) compared with 30 Gy in 5 fractions. Expression of CCL11 and IL-5, which are significant factors in eosinophil recruitment, began increasing at 4 weeks and peaked at 6 weeks after irradiation, paralleling the pattern of eosinophil recruitment. The induction of mast cells, which also play an important role in eosinophil-mediated Th2 immunity,³⁰ was quantified with toluidine blue. The number of mast cells per 400×

microscopic field in the infiltrated dermal area remained higher following 30 Gy in single fraction compared with 30 Gy in 5 fractions (Fig. 10d). Expression of IL-13, which is known to be capable of driving tissue fibrosis,¹⁷ increased over time and was also more pronounced after single-fraction compared with fractionated irradiation of 30 Gy (Fig. 10e).

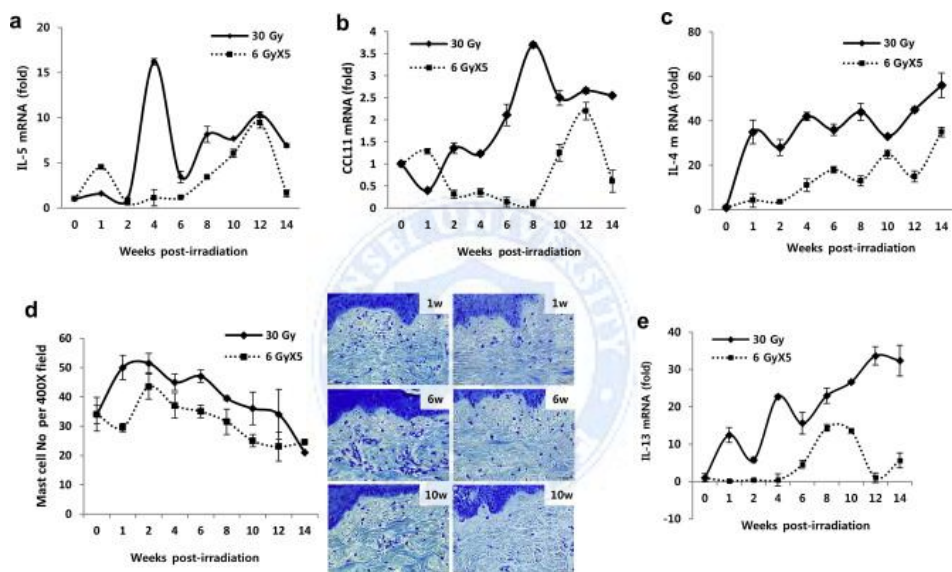


Figure 10. Upregulation of eosinophil-related factors in porcine skin by 30 Gy in single fraction vs. 30 Gy in 5 fractions. mRNA was isolated from biopsy specimens, and qRT-PCR was performed with target primers. β -actin-normalized mRNA levels of (a) IL-5, (b) CCL11, (c) IL-4, (d) number of mast cells (stained with toluidine blue and counted per 400 \times field), and (e) IL-13 mRNA level in porcine skin after 30 Gy in single fraction vs. 5 fractions.

C. IL-33 induction in mouse skin following 30 Gy in single-fraction

To identify factors that promote eosinophil recruitment in irradiated skin, we performed RNA sequencing (RNA-Seq) in irradiated mouse skin. RNA-Seq analysis using DESeq identified 679 differentially expressed genes (DEGs) (333 upregulated, 346 downregulated) in irradiated mouse skin samples. Ingenuity Pathway Analysis of diseases and functions for the 333 upregulated DEGs showed that these were significantly related with eosinophil adherence ($P < 0.003$), immune cell adherence ($P < 0.001$), or vascular endothelial cell chemotaxis ($P < 0.0001$). Related genes and functions are summarized in Figure 11a. Consistent with phenotypic changes, fifth complement component (C5), chemokine (C-X-C motif) receptor 2 (CXCR2), alpha 5-integrin (ITGA5), P-selectin (SELP), and IL-1, which are involved in immune response; eosinophil recruitment; and vascular endothelial cell chemotaxis, were upregulated, and canonical pathway analysis revealed enrichment of the granulocyte adhesion and diapedesis pathways in the DEGs of 30-Gy-irradiated mouse skin (Figure 11b). IL-1R signaling plays a central role in the regulation of immune and inflammatory responses. IL-1, IL-18/IL-37, IL-33, and IL-36/IL-38 are among the IL-1 family members that share the IL-1R α chain.³¹ Therefore, we searched the DEGs for IL-1 family genes and found that IL-1, IL-18, and IL-33 were upregulated DEGs in 30 Gy-irradiated mouse skin (Fig. 11c). IL-33 had the highest fold-change (> 7 folds) among IL-1 family genes, consistent with recent reports that IL-33 is expressed in endothelial and epithelial barrier tissues, such as skin and vessels, that play important roles in

the response to vascular damage and infection.^{32,33} In mice, IL-33 is not expressed constitutively in normal blood vessels.³⁴ However, damaged vascular endothelial cells and tissue in an ApoE (-/-) atherosclerosis mouse model produce high IL-33 levels.³⁵ We validated the IL-33 mRNA upregulation using qRT-PCR, which indicated 4-fold higher IL-33 mRNA levels in 30 Gy-irradiated mouse skin than non-irradiated skin (Figure 11d). Moreover, expression of IL-33 mRNA and the IL-33 receptor ST2 was more significantly elevated in porcine skin 1 week after 30 Gy in single fraction compared with 30 Gy in 5 fractions (Figure 11e). These results indicate that high-dose-per-fraction irradiation induces IL-33 production in the early period (1-2 weeks after irradiation) and may be accompanied by vascular endothelial cell damage.

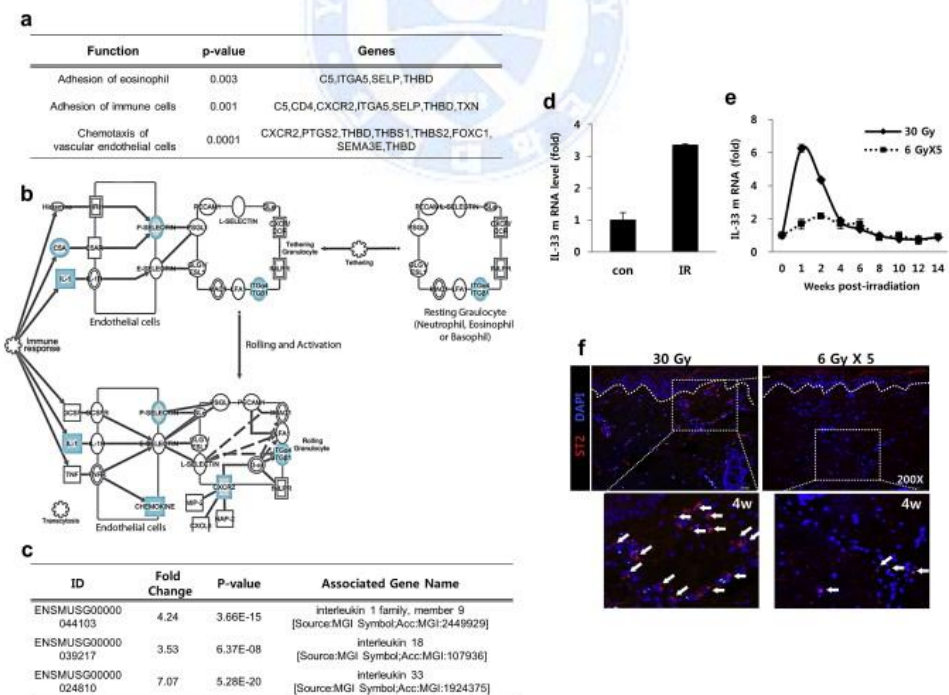


Figure 11. Enrichment of granulocyte adhesion and upregulation of IL-33. Ingenuity Pathway Analysis was conducted using differentially expressed genes (DEGs; $P < 0.01$, Bonferroni corrected) in mouse skin with or without irradiation of 30 Gy in single fraction. (a) Enrichment of granulocyte adhesion molecules and (b) diapedesis pathways by canonical pathway analysis and (c) IL-1 family genes including IL-1, 18, and 33 were among the upregulated DEGs. (d) IL-33 mRNA levels determined by qRT-PCR in 30 Gy-irradiated mouse skin. Porcine skin was irradiated with 30 Gy in a single fraction or 5 fractions and biopsied at the indicated times. (e) IL-33 mRNA levels determined by qRT-PCR in irradiated porcine skin and (f) ST2 receptor expression in irradiated porcine skin biopsied at 4 weeks after irradiation and stained with ST2 antibody (red).

D. Eosinophil-mediated Th2 immune reaction by IL-33 secreted from impaired vascular endothelial cells in the skin

Since ablative, hypofractionated radiotherapy, which delivers over 10 Gy per fraction, have been reported to induce vascular damage,³⁶ microvessel density was assessed by CD31 staining. The density of dermal microvessels in porcine skin was lower during the early period (0-6 weeks) after 30 Gy in single fraction (Fig. 12a). To identify vascular damage induced by irradiation, biopsy specimens from irradiated porcine skin were co-stained with p53-binding protein 1 (P53BP1), which is a classic DNA damage response marker, and CD31 antibodies. The number of p53BP1 and CD31 double-positive cells was greater in skin irradiated

with 30 Gy in single fraction than 30 Gy in 5 fractions (Figure 12b).

Next, we investigated whether IL-33 is secreted from dermal blood vessels upon irradiation. Since no IL-33 antibody was available for immunofluorescence staining of porcine skin, we used irradiated mouse skin for IL-33 and CD31 co-staining. IL-33 expression was significantly increased in dermal vessels after 30 Gy in single fraction compared with the control (Figure 12c). To identify whether IL-33 is released from damaged vascular endothelial cells by radiation in vitro, we used HUVECs and set 12 Gy- and 4 Gy- irradiated cells as the counterparts of the skin irradiated with 30 Gy in single fraction and 30 Gy in 5 fractions in vivo, respectively. Culture media were collected 48 h after irradiation to measure IL-33 synthesis. The mRNA and protein levels of IL-33 were increased by radiation in a dose-dependent manner (Figure 12d-e). We also evaluated immune cell recruitment and cytokine release via IL-33-mediated immune responses in a human monocyte co-culture system. The migration of THP-1 cells co-cultured with 12 Gy-irradiated HUVECs was enhanced compared with those cultured with unirradiated HUVECs (Figure 12f). This enhanced THP-1 cell migration and production of IL-4 and IL-6 were impaired by anti-IL-33 antibody treatment (Figure 12f-h), suggesting that endothelial cells impaired by high-dose radiation in single fraction could produce IL-33, which may encourage immune responses such as inflammation and immune cell recruitment.

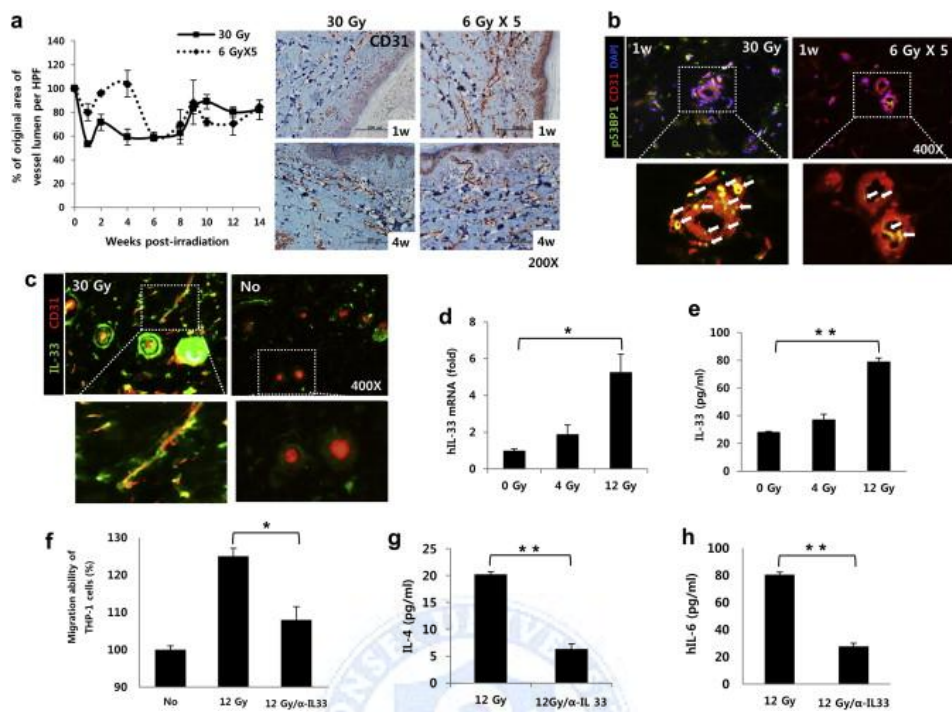


Figure 12. Production of IL-33 and blood vessel damage by high-dose irradiation in single fraction. (a) Mean density of CD31-stained small arterioles, determined by summing the luminal areas of microvessels, in 5 high-power fields ($\times 400$) from sections of each biopsy specimen, expressed as a percentage of the baseline value obtained on Day 0. (b) Co-staining with p53-binding protein 1 (p53BP1, green) and CD31 (red) antibodies demonstrates blood vessel damage in the porcine skin (blue, DAPI nuclear stain; original magnification, $\times 400$) biopsied 1 week after 30 Gy in a single- or 5-fractions. (c) IL-33 secretion from blood vessels in 30 Gy-irradiated or unirradiated mouse skin co-stained with IL-33 (green) and CD31 (red) antibodies (original magnification, $\times 400$). IL-33 (d) mRNA and (e) production in HUVECs irradiated with 0, 4, or 12 Gy and incubated for 48 h.

IL-33 inhibition by anti-IL-33 antibody led to (f) downregulation of THP-1 cell migration in transwell plates after 36-h incubation with 12 Gy-irradiated HUVEC-conditioned culture medium and decreased levels of (g) IL-4 and (h) IL-6 in culture medium 48-h after co-culturing 12-Gy-irradiated HUVECs and THP-1 cells.



IV. DISCUSSION

Radiation-induced skin changes typically follow well-defined stages of progression and have been subdivided into various classifications systems.^{37,38}

Acute and late radiation morbidity scoring by RTOG is one of the most commonly used criteria for radiation induced toxicity. However, the first sign of skin toxicity by RTOG is follicular, faint or dull erythema, which is often observed several weeks into radiation treatment. Currently, there are no effective methods to assess the early changes in the skin and help predict the timing and magnitude of gross skin reaction due to high dose irradiation.

Early radiation effects typically result from the loss of the rapidly proliferating basal epithelial stem cells.³⁹ Within the first week of radiation, some patients may develop a transient erythema, caused by an inflammatory response leading to capillary vasodilatation, increased vascular permeability, and edema.^{39,40} Erythema demarcating the radiation field begins in the second or third week of conventionally fractionated radiation (10-20 Gy) and becomes progressively more evident by the third and fourth week of treatment.³⁷ If the total dose to the skin does not exceed 30 Gy, the dry desquamation phase will typically occur in the fourth or fifth week of radiation.⁴¹ If the total delivered dose is > 40 Gy, the erythema phase may be followed by the moist desquamation phase, which has similar histologic features to a second-degree burn.³⁷

Vascular endothelial cells are the primary target in late radiation-induced skin injuries, leading to dermal fibrosis, although endothelial cell damage begins

as early as the acute phase skin reaction. We showed that skin damage, indicated by decreased microvessel density, began soon after a transient rise at 1 week, and the damage was most severe at 4-6 weeks post-irradiation, after which the recovery process began. The skin irradiated with 15-30 Gy continued to recover from radiation-induced injury, while skin irradiated with 50-75 Gy was unable to recover fully because the initial damage was too severe. This resembles a consequential late complication in fractionated radiotherapy, which is a late effect consequent to a persistent severe early effect.³⁹ In a previous investigation, pig dorsal skin irradiated with single fractional electron beams of 16 Gy, 18 Gy, and 20 Gy showed a similar pattern of changes in the microvessel density.⁴² In this experiment, the nadir was reached at 7 weeks post-irradiation, with a higher radiation dose resulting in a lower nadir. In our study, the density curves of high dose radiation (50 Gy and 75 Gy) showed lower nadirs appearing earlier than those of low dose radiation (15 and 30 Gy). We used significantly higher radiation doses compared with the doses used in previous works, and it appears that the higher dose caused earlier skin damage that took longer to heal.

Gross skin changes according to RTOG criteria in Figure 3A showed clear dose dependence of radiation-induced skin damage. Although significant changes in the gross skin were not detected during the first 4 weeks after irradiation, eosinophil counts began rising as early as 1 week after irradiation. Changes in the eosinophil counts showed dose-dependent relationships during the first 4 weeks: eosinophil counts began rising soon after irradiation of 75 Gy while

15 Gy-irradiation did not cause increase in eosinophil counts until the 4th week. For the changes in microvessel density, the nadirs for 50 Gy and 75 Gy appeared earlier than those for 15 Gy and 30 Gy, and the level of microvessel density indicated recovery from radiation damage at 12 weeks after 15 Gy and 30 Gy, but not after 50 Gy and 75 Gy. There is a clear difference in gross skin reactions as well as changes at histologic and microscopic levels between irradiation of 15-30 Gy and irradiation of 50-75 Gy. We determined a single fraction of 30 Gy to be the maximum tolerable dose that our pig skin model could tolerate without irreversible skin damage.

In the early stages of endothelial cell damage, leukocytes infiltrate into the irradiated tissue and induce inflammatory responses and early fibrotic changes through secretion of various cytokines including TGF- β and IL-6.⁴ The process of late fibrosis mediated by endothelial cell damage is not clearly understood. Eosinophil granules contain fibrogenic molecules, including TGF- β , IL-4, IL-6, TNF- α , eosinophil cationic protein, and major basic protein. It had been demonstrated that eosinophils act as direct modulatory cells in fibroblast proliferation, collagen synthesis, and lattice contraction, in part through TGF- β .⁸ In Phase I study, eosinophils began appearing at 2 weeks, increased rapidly in number at 4 weeks, peaked at 6-9 weeks, and disappeared 12 weeks after irradiation. This pattern is closely followed by the level of TGF- β 1 expression in the Western-blot analysis, which was detected 1 week after irradiation and continued to increase afterward. Unlike normal wound healing where feedback

mechanisms tightly regulate activation of fibroblasts into myofibroblasts and in turn proliferation and deposition of the collagen matrix, fibrosis is characterized by sustained activation of myofibroblasts through abnormal production of stimulating factors, particularly of TGF- β 1. TGF- β 1 is considered a master switch for the fibrotic changes of the skin after exposure to radiation.⁴³ Martin et al. found that the TGF- β 1 mRNA level was increased in the irradiated skin during the early erythematous phase, which started 3 weeks after irradiation, as well as during the later phases of fibrosis, from 6 to 12 months after irradiation. They suggested that TGF- β 1 is one of the key cytokines involved in the cascade of events that leads to radiation-induced fibrosis, at both early and late stages.⁴⁴ The roles of eosinophils and cytokines produced from eosinophil degranulation, including TGF- β 1, in radiation-induced fibrosis are unclear. Nonetheless, the active transition in the molecular environment of the skin during the latency period including microvessel density, eosinophil level, and the level of TGF- β 1 and IL-6 provides grounds for early intervention for the prevention and treatment of radiation-induced skin injury.

High dose irradiation decreases tumor microvascular density and CD68+ tumor-associated macrophages in irradiated tumors.⁴⁵ Vascular endothelial cells appear to be one of the main targets of hypofractionated radiotherapy in the ablative-dose range used in stereotactic body radiotherapy or radiosurgery (> 10 Gy per fraction).³⁶ However, changes in the tumor micro-environment after hypofractionated radiotherapy and the impact of varying fraction size are not well

understood. In our Phase II study, 30-Gy in single fraction induced more pronounced reduction in vessel density and increase of eosinophil infiltration compared to 30 Gy in 5 fractions. RNA-Seq analysis of irradiated mouse skin showed elevation of chemotaxis-associated factors of vascular endothelial cells. Expression of the IL-1 cytokine family member IL-33 (also known as IL-1F11 and NF-HEV) was markedly increased. Furthermore, increases in IL-33 mRNA and the IL-33 receptor ST2 were more pronounced in pig skin during the early period (1 week) after 30 Gy in single fraction compared with 30 Gy in 5 fractions. We also demonstrated that blocking IL-33 inhibited IL-4 and IL-6 secretion in a co-culture system with THP-1 cells and irradiated HUVECs. Since IL-33 is expressed in various cell types,^{32,46,47} it may have been produced in other skin cells such as dermal fibroblasts, mast cells, or lymphocytes in this study. However, IL-33 mRNA and ST-2 expression were sharply increased at 1 week after high-dose irradiation of porcine skin, indicating that IL-33 induction was increased as an early response. The acute effect of radiation on blood vessels is an important trigger, and vascular endothelial cells are a primary target for killing tumor cells in hypofractionated ablative radiotherapy compared with conventional fractionation. Therefore, in the current study, IL-33 induction in vascular endothelial cells triggered by high-dose radiation may have acted as an immune modulator and caused recruitment of eosinophils in the irradiated site. Additionally, since IL-33 is a chemo-attractant of Th2 cells, enhanced production of IL-4, IL-5, and IL-13 can stimulate Th2 immune responses such as mast cell

activation via IgE-dependent immune reactions. Thus, IL-33 could also act on mast cells that in turn induce Th2 immune response, resulting in eosinophil recruitment.

Eosinophils release Th2-type cytokines and act as direct regulators of fibroblast proliferation and collagen synthesis, in part through TGF- β .⁸ Such eosinophil-produced soluble factors can act as autocrine signals through engagement of cytokine receptors in eosinophils.⁴⁸ In the present study, upregulation of eosinophil-mediated Th2 cytokines was more pronounced with single-fraction high-dose irradiation compared with a multiple-fraction schedule, which also affected the degree of eosinophil recruitment. Eosinophil-mediated profibrotic factors such as IL-13 and TGF- β may in turn affected fibrotic responses such as collagen accumulation and α -SMA expression.

High-dose radiation in single fraction can induce more pronounced disruption of vascular endothelial cell function compared with the same dose of radiation in fractionated schedule. Vascular endothelial cells damaged by high-dose radiation secrete IL-33, which may stimulate fibrotic responses via eosinophil recruitment and eosinophil-mediated Th2 immune responses in irradiated skin (Figure 12).

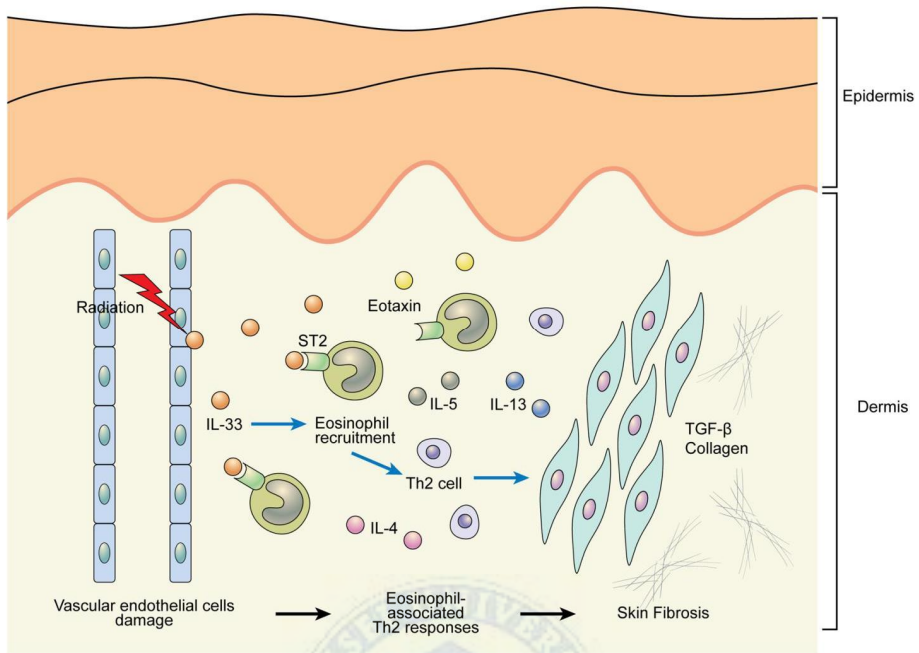


Figure 13. Schematic model of the signaling pathway involved in the eosinophil-mediated immune response and fibrosis induced by high-dose radiation in the skin.

We have not shown a direct causal relationship between increased production of IL-33 after high-dose-per-fraction radiation and induction of skin fibrosis, and there may be multiple steps involved. Nonetheless, we have shown that IL-33 can be a key factor in eosinophil-mediated fibrosis in hypofractionated radiotherapy, and IL-33 may be a useful indicator in predicting common complications such as fibrosis in cancer patients treated with radiotherapy.

V. CONCLUSION

We established a time-dose response relationship for the skin exposed to high-dose radiation in single fraction. Although it is a common practice to divide radiation-induced normal tissue injury into acute and late phases, it is clearly evident that response to radiation is not a combination of discrete and unrelated episodes but rather a continuous course of interrelated events. Our porcine skin model revealed that the early latency period after high dose irradiation is not a static phase suggested by the lack of gross changes but rather an active period during which many molecular events are in progress.

Vascular endothelial cells damaged by high-dose radiation secrete IL-33, which may stimulate fibrotic responses via eosinophil recruitment and eosinophil-mediated Th2 immune responses in irradiated skin. IL-33 can be a key factor in eosinophil-mediated fibrosis in hypofractionated ablative radiotherapy, and IL-33 may be a useful factor to predict common complications such as fibrosis in cancer patients treated with radiotherapy.

REFERENCES

1. Hepel JT, Tokita M, MacAusland SG, Evans SB, Hiatt JR, Price LL, et al. Toxicity of Three-Dimensional Conformal Radiotherapy for Accelerated Partial Breast Irradiation. *International Journal of Radiation Oncology*Biology*Physics* 2009;75:1290-6.
2. Hoppe BS, Laser B, Kowalski AV, Fontenla SC, Pena Greenberg E, Yorke ED, et al. Acute skin toxicity following stereotactic body radiation therapy for stage I non-small-cell lung cancer: who's at risk? *International journal of radiation oncology, biology, physics* 2008;72:1283-6.
3. Archambeau JO, Pezner R, Wasserman T. Pathophysiology of irradiated skin and breast. *International journal of radiation oncology, biology, physics* 1995;31:1171-85.
4. Lawenda BD, Johnstone PA. Skin. In: Shrieve DC, Loeffler JS, editors. *Human Radiation Injury*. Philadelphia, PA: Lippincott Williams & Wilkins; 2011. p.499-515.
5. Chen Y, Williams J, Ding I, Hernady E, Liu W, Smudzin T, et al. Radiation pneumonitis and early circulatory cytokine markers. *Seminars in Radiation Oncology* 2002;12:26-33.
6. Rubin P, Johnston CJ, Williams JP, McDonald S, Finkelstein JN. A perpetual cascade of cytokines postirradiation leads to pulmonary fibrosis. *International Journal of Radiation Oncology*Biology*Physics* 1995;33:99-109.
7. Wangoo A, Sparer T, Brown IN, Snewin VA, Janssen R, Thole J, et al. Contribution of Th1 and Th2 cells to protection and pathology in experimental models of granulomatous lung disease. *The journal of immunology* 2001;166:3432-9.
8. Levi Schaffer F, Garbuzenko E, Rubin A, Reich R, Pickholz D, Gillery

- P, et al. Human eosinophils regulate human lung- and skin-derived fibroblast properties in vitro: a role for transforming growth factor beta (TGF-beta). *Proceedings of the National Academy of Sciences of the United States of America* 1999;96:9660-5.
9. Spencer LA, Weller PF. Eosinophils and Th2 immunity: contemporary insights. *Immunology and cell biology* 2010;88:250-6.
 10. Chiamonte MG, Mentink-Kane M, Jacobson BA, Cheever AW, Whitters MJ, Goad ME, et al. Regulation and function of the interleukin 13 receptor alpha 2 during a T helper cell type 2-dominant immune response. *The Journal of experimental medicine* 2003;197:687-701.
 11. Opal SM, DePalo VA. Anti-inflammatory cytokines. *Chest* 2000;117:1162-72.
 12. Chiamonte MG, Cheever AW, Malley JD, Donaldson DD, Wynn TA. Studies of murine schistosomiasis reveal interleukin-13 blockade as a treatment for established and progressive liver fibrosis. *Hepatology* 2001;34:273-82.
 13. Rank MA, Kobayashi T, Kozaki H, Bartemes KR, Squillace DL, Kita H. IL-33-activated dendritic cells induce an atypical TH2-type response. *Journal of Allergy and Clinical Immunology* 2009;123:1047-54.
 14. Louten J, Rankin AL, Li Y, Murphy EE, Beaumont M, Moon C, et al. Endogenous IL-33 enhances Th2 cytokine production and T-cell responses during allergic airway inflammation. *International Immunology* 2011;23:307-15.
 15. Schmitz J, Owyang A, Oldham E, Song Y, Murphy E, McClanahan TK, et al. IL-33, an interleukin-1-like cytokine that signals via the IL-1 receptor-related protein ST2 and induces T helper type 2-associated cytokines. *Immunity* 2005;23:479-90.
 16. Li D, Guabiraba R, Besnard AG, Komai-Koma M, Jabir MS, Zhang L, et al. IL-33 promotes ST2-dependent lung fibrosis by the induction of

- alternatively activated macrophages and innate lymphoid cells in mice. *Journal of allergy and clinical immunology* 2014;134:1422-32.e11.
17. Rankin AL, Mumm JB, Murphy E, Turner S, Yu N, McClanahan TK, et al. IL-33 induces IL-13-dependent cutaneous fibrosis. *The journal of immunology* 2010;184:1526-35.
 18. Cox JD, Stetz J, Pajak TF. Toxicity criteria of the Radiation Therapy Oncology Group (RTOG) and the European Organization for Research and Treatment of Cancer (EORTC). *International journal of radiation oncology, biology, physics* 1995;31:1341-6.
 19. Draaijers LJ, Tempelman FR, Botman YA, Kreis RW, Middelkoop E, van Zuijlen PP. Colour evaluation in scars: tristimulus colorimeter, narrow-band simple reflectance meter or subjective evaluation? *Burns* 2004;30:103-7.
 20. Lamme EN, de Vries HJ, van Veen H, Gabbiani G, Westerhof W, Middelkoop E. Extracellular matrix characterization during healing of full-thickness wounds treated with a collagen/elastin dermal substitute shows improved skin regeneration in pigs. *The journal of histochemistry and cytochemistry* 1996;44:1311-22.
 21. Rasband W. ImageJ. <http://imagej.nih.gov/ij/2012/>
 22. Kim JW, Lee DW, Choi WH, Jeon YR, Cho H, Hong ZY. Development of a porcine skin injury model and characterization of the dose-dependent response to high-dose radiation. *JOURNAL OF RADIATION RESEARCH* 2013;54:823-31.
 23. Yoo H, Kang JW, Lee DW, Oh SH, Cho J. Pyruvate metabolism: A therapeutic opportunity in radiation-induced skin injury. *Biochemical and biophysical research communications* 2015;460:504-10.
 24. Ma CM, Coffey CW, DeWerd LA, Liu C, Nath R, Seltzer SM, et al. AAPM protocol for 40-300 kV x-ray beam dosimetry in radiotherapy and radiobiology. *Medical physics* 2001;28:868-93.

25. Andrews S. FastQC: A quality control tool for high hroughput sequence data. Reference Source; 2010.
26. Trapnell C, Pachter L, Salzberg SL. TopHat: discovering splice junctions with RNA-Seq. *Bioinformatics* 2009;25:1105-11.
27. Li H, Handsaker B, Wysoker A, Fennell T, Ruan J, Homer N, et al. The Sequence Alignment/Map format and SAMtools. *Bioinformatics* 2009;25:2078-9.
28. Anders S. HTSeq: Analysing High-throughput Sequencing Data with Python. Available at <http://www-huber.embl.de/users/anders/HTSeq/doc/overview.html>
29. Anders S. Analysing RNA-Seq data with the DESeq Package. *Mol. Biol.*; 2010.
30. Stone KD, Prussin C, Metcalfe DD. IgE, mast cells, basophils, and eosinophils. *Journal of allergy and clinical immunology* 2010;125:S73-80.
31. Lopetuso LR, Chowdhry S, Pizarro TT. Opposing Functions of Classic and Novel IL-1 Family Members in Gut Health and Disease. *Frontiers in Immunology* 2013;4:181.
32. Moussion C, Ortega N, Girard JP. The IL-1-like cytokine IL-33 is constitutively expressed in the nucleus of endothelial cells and epithelial cells in vivo: a novel 'alarmin'? *PLoS ONE* 2008;3:e3331.
33. Tajima S, Oshikawa K, Tominaga S, Sugiyama Y. The increase in serum soluble ST2 protein upon acute exacerbation of idiopathic pulmonary fibrosis. *Chest* 2003;124:1206-14.
34. Pichery M, Mirey E, Mercier P, Lefrancais E, Dujardin A, Ortega N, et al. Endogenous IL-33 is highly expressed in mouse epithelial barrier tissues, lymphoid organs, brain, embryos, and inflamed tissues: in situ analysis using a novel Il-33-LacZ gene trap reporter strain. *The journal of immunology* 2012;188:3488-95.

35. Miller AM, Xu D, Asquith DL, Denby L, Li Y, Sattar N, et al. IL-33 reduces the development of atherosclerosis. *The Journal of experimental medicine* 2008;205:339-46.
36. Park HJ, Griffin RJ, Hui S, Levitt SH, Song CW. Radiation-induced vascular damage in tumors: implications of vascular damage in ablative hypofractionated radiotherapy (SBRT and SRS). *Radiation Research* 2012;177:311-27.
37. Fajardo L. *Skin Pathology of Radiation Injury*. New York: Masson Publishing; 1982.
38. Tessmer C. *Radiation effects in skin*. Baltimore: Williams & Wilkins; 1971.
39. Hall E. *Radiobiology for the Radiobiologist*. 7th edition ed. Philadelphia: Lippincott Williams & Wilkins; 2012.
40. Jolles B, Harrison RG. Enzymic processes and vascular changes in the skin radiation reaction. *British journal of radiology* 1966;39:12-8.
41. Rubin P, Casarett G. *Clinical Radiation Pathology*. Philadelphia: W.B Saunders; 1968.
42. Hadad I, Johnstone BH, Brabham JG, Blanton MW, Rogers PI, Fellers C, et al. Development of a porcine delayed wound-healing model and its use in testing a novel cell-based therapy. *International journal of radiation oncology, biology, physics* 2010;78:888-96.
43. Martin M, Lefaix J, Delanian S. TGF-beta1 and radiation fibrosis: a master switch and a specific therapeutic target? *International journal of radiation oncology, biology, physics* 2000;47:277-90.
44. Martin M, Lefaix JL, Pinton P, Crechet F, Daburon F. Temporal modulation of TGF-beta 1 and beta-actin gene expression in pig skin and muscular fibrosis after ionizing radiation. *Radiation Research* 1993;134:63-70.
45. Chen FH, Chiang CS, Wang CC, Tsai CS, Jung SM, Lee CC, et al.

Radiotherapy decreases vascular density and causes hypoxia with macrophage aggregation in TRAMP-C1 prostate tumors. *Clinical cancer research* 2009;15:1721-9.

46. Sponheim J, Pollheimer J, Olsen T, Balogh J, Hammarström C, Loos T, et al. Inflammatory bowel disease-associated interleukin-33 is preferentially expressed in ulceration-associated myofibroblasts. *The American journal of pathology* 2010;177:2804-15.
47. Hsu CL, Bryce PJ. Inducible IL-33 expression by mast cells is regulated by a calcium-dependent pathway. *The journal of immunology* 2012;189:3421-9.
48. Rothenberg ME, Hogan SP. THE EOSINOPHIL. *Annual Review of Immunology* 2006;24:147-74.



ABSTRACT (IN KOREAN)

동물 모델을 통한 고 분할선량 방사선 유도 피부손상의 특징
분석 및 호산구 매개 피부 섬유화 기전 규명 연구

<지도교수 조재호>

연세대학교 대학원 의학과

김 준 원

소분할 절제방사선치료 (hypofractionated ablative radiotherapy)에 대한 정상조직의 반응은 통상분할 방사선치료에 의한 조직반응과 차이를 보인다. 본 연구에서는 동물모델을 이용하여 고 분할선량 (high-dose-per-fraction) 방사선치료에 대한 선량의존 피부반응의 특성을 확인하고 호산구 매개 피부섬유화의 기전을 규명하고자 하였다. 1단계 연구에서는 미니돼지의 등쪽 피부를 네 부위로 나누고 6 MeV 전자선을 사용해 각각 15 Gy, 30 Gy, 50 Gy, 75 Gy를 1회 조사하였다. 방사선 조사 후 피부의 육안적 변화는 분광광도계 (spectrophotometer)를 통해 정량화 하였고 12주 관찰기간 동안 주기적으로 피부 전층 생검을 통해 조직 변화를 관찰하였다. 또한 CD-31 면역염색을 통해 피부 혈관

밀도의 변화와 Western blot을 통해 IL-6와 TGF- β 1의 발현 정도를 관찰하였다. 방사선 조사 후 4주간 잠재기 (latency period)를 거쳐 홍반화 (erythema), 건성 표피탈락 (dry desquamation), 습성 표피탈락 (wet desquamation), 궤양 (ulceration) 형성이 관찰되었고, 50 Gy 이상 조사된 부위에서 비가역적인 피부궤양과 괴사가 관찰되었다. 생검 조직에서는 방사선조사 4주 후부터 호산구 수의 급격한 증가가 관찰되었고 7-8주에 최대치에 이른 후 정상화되었다. 피부혈관 밀도는 방사선조사 후 1주에 일시적 증가를 보였고 4-6주에 최저치에 도달했으며 9주에 최대 회복을 보였다. IL-6와 TGF- β 1은 방사선조사 후 초기부터 증가하는 것이 관찰되었다. 2단계 연구에서는 미니돼지의 피부를 두 부위로 나누어 각 부위에 30 Gy를 1회와 5회에 나누어 조사하였고 정량화 실시간 중합효소연쇄반응 (quantitative real time PCR, qRT-PCR) 을 통해 호산구 관련 Th-2 사이토카인의 변화를 분석하였다. 또한, 30 Gy 조사된 마우스 피부조직의 RNA sequencing과 THP-1 세포와 방사선 조사된 HUVEC의 공동배양 시스템을 이용한 기능분석을 통해 호산구 매개 피부 섬유화 기전을 조사하였다. 30 Gy가 1회 조사된

조직에서 5회에 나누어 조사된 조직에 비해 호산구 증가, collagen, TGF- β 같은 섬유화 유도 인자의 발현, IL-4, IL-5, CCL11, IL-13, IL-33 같은 호산구 관련 사이토카인의 증가, 그리고 피부혈관 밀도의 감소가 현저히 증가된 것이 관찰되었다. 30 Gy 조사된 돼지와 마우스의 피부, 그리고 12 Gy 조사된 HUVEC에서 IL-33 발현이 유의하게 증가하였고 IL-33을 차단했을 때 THP-1 세포/HUVEC 공동배양 시스템에서 THP-1 세포의 이동능력과 사이토카인 분비가 억제된 것을 관찰할 수 있었다. 본 연구에서는 돼지피부 모델이 고 분할선량 방사선조사로 인한 피부손상 연구의 효과적인 모델임을 확인할 수 있었고, 고 분할선량 조사로 인해 호산구 매개 피부 섬유화 반응이 증폭되고 여기에는 IL-33이 핵심인자로 작용함을 확인할 수 있었다.

핵심되는 말: 방사선유도 피부손상; 돼지 피부손상 모델; 고 분할선량 조사, 호산구 매개 섬유화; IL-33

PUBLICATION LIST

Kim JW, Lee DW, Choi WH, Jeon YR, Cho H, Hong ZY. Development of a porcine skin injury model and characterization of the dose-dependent response to high-dose radiation. JOURNAL OF RADIATION RESEARCH 2013;54:823-31.

Lee EJ, Kim JW, Yoo H, Kwak W, Choi WH, Cho S, Choi YJ, Lee YJ, Cho J. Single high-dose irradiation aggravates eosinophil-mediated fibrosis through IL-33 secreted from impaired vessels in the skin compared to fractionated irradiation. BIOCHEMICAL AND BIOPHYSICAL RESEARCH COMMUNICATIONS 2015;464:20-6.

